Self-consistent diverted tokamak equilibria with nonzero edge current*

Shi Bing-Ren(石秉仁)†

Southwestern Institute of Physics, Chengdu 610041*, China*

(Received 1 August 2011; revised manuscript received 2 September 2011)

The semi-analytical method, previously used to construct model double-null and single-null diverted tokamak equilibria (Bingren Shi, *Plasma Phys. Control Fusion* **50** (2008) 085006, **51** (2009) 105008, *Nucl. Fusion* **51** (2011) 023004), is extended to describe diverted tokamak equilibria with nonzero edge current, including the Pfirsch–Schlüter(PS) current. The PS current density is expressed in a way suitable to describe a diverted tokamak configuration in the near separatrix region. The model equilibrium is expressed by only two terms of the exact separable solutions of the Grad–Shafranov equation, one of which is governed by a homogeneous ordinary differential equation, and the other by an inhomogeneous one. The particular merits of such a model configuration are that the internal region inside the separatrix and a suitable scrape-off layer can be simultaneously described by this exact solution. To investigate the physics in the region near the X-point, the magnetic surfaces can be satisfactorily described by approximate hyperbolic curves.

Keywords: diverter configuration, nonzero edge current, PS current

PACS: 52.55.Fa, 52.55.Rk **DOI:** 10.1088/1674-1056/21/4/045203

1. Introduction

The physics in the near separatrix region of diverted tokamak plasmas is very important for the interpretation of mode transition from the low confinement regime (L-mode) to the high confinement regime (H-mode).[1] As is well known, the H-mode is characterized by edge localized modes (ELMs), and these modes are excited by the pressure gradient in the pedestal region and the nonzero edge current at the separatrix.[2] Theoretically, we hope to obtain a self-consistent equilibrium with nonzero edge current, then we can calculate the stability criterion more accurately. Previously, we provided a semi-analytic approach[3−5] for constructing exact model diverted tokamak or spherical tokamak (ST) configurations with zero edge current. In this paper, we extend this method to the case with a proper edge current. Therefore, to become compatible with the peeling-ballooning type instability studies, an exact equilibrium configuration consistent with a suitable edge current is hoped for. In this situation, the corresponding Grad–Shafranov equation becomes inhomogeneous[6,7] and we need to extend our method, which was originally suitable for solving the homogeneous equation, to find exact solutions. The simplest case for the nonzero edge current equilibrium is the Solovév-type one,[8−14] which corresponds to a quasi-uniform current profile and has been extensively studied for non-diverted configurations[8−11] and also for recently reported diverted configurations.[12−14] In Ref. [12], a diverted tokamak equilibrium with an internal null point was described by the Solovév-type solution, and this equilibrium has a suitable inboard scrape-off layer (SOL) region. Recently, analytic ITER-like diverted tokamak and spherical torus configurations were given by the so-called "one size fits all" approach for the quasi-uniform current profile[14] that corresponds to an internal region solution. Also recently, symmetric (double-null) and asymmetric (single-null) diverted tokamak equilibria were constructed by Solovév-type solutions[15] to describe the internal region of a tokamak plasma. For the non-uniform current profile with nonzero edge current, analytic solutions were obtained in Refs. [6] and [7]. Thus the obtained solutions that generally consist of many terms of separable solutions involving some known special functions, such as the Bessel,[6] the hypergeometric,[7] and the Whittaker[16] functions etc., are limited to non-diverted configurations and only the internal region is described. In this paper, we consider double-null diverted tokamak equilibria with non-uniform current profiles and nonzero edge currents. In this case, to

*Project supported by the National Magnetic Confinement Fusion Science Program of China (Grant No. 2009GB101002).

†Corresponding author. E-mail: Shibr@swip.ac.cn

© 2012 Chinese Physical Society and IOP Publishing Ltd

obtain a solution that can describe both the internal region and a suitable SOL region, we still use the semi-analytic approach[3−5] to make it possible to construct model diverted tokamak or ST configurations by only two terms of separable solutions like the following (in cylindrical coordinates):

$$\Psi(R,Z) = f(R)\cos kZ + g(R), \tag{1}$$

where functions $f(R)$ and $g(R)$ satisfy the corresponding ordinary differential equations generated from the Grad–Shafranov equation[3−5] (see below). These equations are solved by a Runge–Kutta solver within a finite range $R_1 \leq R < R_2$. Within this range, there are no singularities for the two differential equations and very accurate solutions can be obtained so that their derivatives with respect to the radial variable R can also be obtained accurately. Then, the separatrix can be determined to very high accuracy. This makes it possible to accurately analyse the stability or transport in the very near separatrix region.

The rest of this paper is organized as follows. In Section 2, the properties of an equilibrium with nonzero edge current are discussed generally and the determination of Pfirsch–Schlüter current in diverted configuration is carried out, and the magnetic averaging of physical quantities method in the very near separatrix region is discussed. In Section 3, the method for the determination of the model equilibrium configurations is outlined. Configurations corresponding to pure PS current and general nonzero edge current are given as examples. In Section 4, we give concluding remarks about the method and the physical results obtained.

2. Model tokamak equilibria with nonzero edge currents

2.1. The Pfirsch–Schlüter current in the diverted tokamak plasma edge

The plasma parameters in the tokamak edge are usually thought to be in the collisional regime, traditionally referred to as the Pfirsch–Schlüter regime,[17] because these authors first analysed particle transport and edge current using the fluid method.[18,19] The parallel component of the edge current density can generally be expressed by the following expression[17−19]

$$j_{\parallel} = -\Big(\frac{p'(\Psi)F}{B}\Big)\Big(1 - \frac{B^2}{\langle B^2\rangle}\Big) + \frac{\langle E_\zeta B_\zeta\rangle B}{\eta\langle B^2\rangle}. \tag{2}$$

In this expression, $\langle A\rangle = \oint A\frac{\mathrm{d}l}{B_\mathrm{p}} / \oint \frac{\mathrm{d}l}{B_\mathrm{p}}$ is an averaged quantity over the magnetic surface considered, B and B_p are the total magnetic strength and the poloidal magnetic field, respectively, $p'(\Psi)$ is the derivative of the plasma pressure with respect to the poloidal flux $\Psi(R,Z)$, and the toroidally symmetric magnetic field is expressed as

$$\boldsymbol{B} = \nabla\Psi \times \nabla\zeta + F\nabla\zeta. \tag{3}$$

The first term on the right-hand side of Eq. (2) is the Pfirsch–Schlüter current, while the second term is the current driven by external electric field. Comparing with the Grad–Shafranov equation

$$\begin{aligned}\Delta^*\Psi &= \frac{\partial^2\Psi}{\partial R^2} - \frac{1}{R}\frac{\partial\Psi}{\partial R} + \frac{\partial^2\Psi}{\partial Z^2}\\ &= -\mu_0 R j_\zeta = -\mu_0 R^2 p'(\Psi) - \frac{1}{2}F^{2\prime}(\Psi),\end{aligned} \tag{4}$$

we note that the toroidal current consists of two terms, one is proportional to the major radius R and the other is inversely proportional to it

$$j_\zeta = Rp'(\Psi) + \frac{1}{2\mu_0 R}F^{2\prime}(\Psi) = a(\Psi)R + \frac{b(\Psi)}{R}. \tag{5}$$

If the poloidal magnetic field is much smaller than the toroidal one, as is true for the tokamak, we have

$$j_\zeta = p'\Big(R - \frac{F^2}{\langle B^2\rangle R}\Big) + \frac{R_*}{R}j_\Omega(\Psi). \tag{6}$$

Here R_* is a reference position. In the above expression, the first term on the right-hand side is the PS current density, while $j_\Omega = F\langle E_\zeta B_\zeta\rangle/(\eta\langle B^2\rangle)$ is the Ohmic current density which we assume is in the same direction as the toroidal magnetic field ($\boldsymbol{B}\cdot\boldsymbol{j} > 0$). Comparing Eq. (6) with Eq. (5), we obtain

$$\begin{aligned}a(\Psi) &= p'(\Psi),\\ b(\Psi) &= \frac{F^{2\prime}}{2\mu_0} = -\frac{p'F^2}{\langle B^2\rangle} + R_* j_\Omega.\end{aligned}$$

The pure PS current case corresponds to $j_\Omega = 0$, and in this case we have $\langle B^2\rangle = F^2/R(X)^2$ with $R(X)$ being the radial position of the X-point. Therefore, it is clear that at the X-point, the PS current density automatically equals zero. Due to this property, we set the reference position the same as that of the X-point: $R_* = R(X)$. In the following, we set $\Psi = 0$ at the plasma boundary (separatrix) and assume that the functions $p(\Psi)$ and $F^2(\Psi)$ have the following forms:

$$p(\Psi) = p_0\Big(\frac{\Psi}{\Psi_a}\Big)^2 + p_1\Big(\frac{\Psi}{\Psi_a}\Big) + p_2, \tag{7}$$

$$F^2(\Psi) = (B_{t0}^2 R_0^2)\Big[1 + \alpha_2\Big(\frac{\Psi}{\Psi_a}\Big)^2 + \alpha_1\Big(\frac{\Psi}{\Psi_a}\Big)\Big]. \tag{8}$$

Then the sum $p_0 + p_1 + p_2$ is the pressure value at the magnetic axis and Ψ_a is the poloidal flux there,

which is also its maximum. For a given set of parameters $(p_0, p_1, \alpha_2, \alpha_1)$, we can separate the PS current from the Ohmic current. For a pure PS current, the following relation is valid

$$\alpha_1 = -\frac{2p_1}{\langle B^2\rangle}. \tag{9}$$

Previously, in Ref. [8], for the same profiles of $p(\Psi)$ and $F(\Psi)$ as in Eqs. (7) and (8), the authors developed an analytical method and obtained two families of exact equilibrium solutions. Usually, these solutions expressed by hypergeometric functions are very complicated, and we need many terms and very accurate numerical coefficients to construct a concrete configuration so that it is hard to use them in stability or transport analysis.

2.2. Average operation over the magnetic surface in the near separatrix region

Now we consider the calculation of averaged physical quantities over the magnetic surface in the near separatrix region, including the separatrix itself. As examples, we consider the safety factor $q(\Psi)$ and the specific volume as defined by

$$\begin{aligned} q(\Psi) &= \frac{F}{2\pi}\oint \frac{\mathrm{d}l}{R|\nabla\Psi|} \\ &= \frac{F}{2\pi}\int_0^{2\pi} \frac{r(\Psi,\theta)\mathrm{d}\theta}{R|\Psi_R\cos\theta + \Psi_Z\sin\theta|}, \end{aligned} \tag{10}$$

$$V'(\Psi) = \oint \frac{\mathrm{d}l}{B_p} = \frac{1}{2\pi}\int_0^{2\pi} \frac{Rr\,\mathrm{d}\theta}{|\Psi_R\cos\theta + \Psi_Z\sin\theta|}. \tag{11}$$

Here, use has been made of the relationship in the local polar coordinates (r,θ): $\mathrm{d}l/B_p = r\,\mathrm{d}\theta/B_\theta$ and $B_\theta = \frac{1}{R}|\Psi_R\cos\theta + \Psi_Z\sin\theta|$.

It is well known that both of these quantities diverge logarithmically approaching the X-point,[20] and the dominant contributions to these quantities are from a short arc near the X-point in their integrals along the magnetic field lines. We can express the flux function near the X-point by its Taylor expansion

$$\begin{aligned} \Psi(R,Z) =& \Psi(X) + \frac{1}{2}\Psi_{RR}(X)(R-R(X))^2 \\ &+ \frac{1}{2}\Psi_{ZZ}(X)(Z-Z(X))^2 \\ &+ \Psi_{RZ}(X)(R-R(X))(Z-Z(X)) + \cdots. \end{aligned} \tag{12}$$

The argument X denotes the coordinates at the X-point, while the subscripts R, Z, RR, ZZ, RZ, represent the partial differentiation with respect to them. Use has been made of the condition $\Psi_R(X) = \Psi_Z(X) = 0$, and we should indicate that in the general case, $\Psi_{RZ}(X) \neq 0$. However, we can suitably rotate the R, Z axes to eliminate the cross term. Here, without loss of generality, we use our simplified diverted configuration expressed by Eq. (1), and in such a case we have $\Psi_{RZ}(X) = 0$. The determinations of Ψ_{RR} and Ψ_{ZZ} will be seen in the concrete applications below. Here we only have a general discussion. We can verify that $\alpha = \frac{1}{2}\Psi_{ZZ}(X) > 0$ while $\Psi_{RR} = -\lambda\alpha < 0$. Then the magnetic surface near the X-point can be written as

$$\begin{aligned} \Psi(R,Z) =& \Psi(X) - \lambda\alpha(R-R(X))^2 \\ &+ \alpha(Z-Z(X))^2 \ldots. \end{aligned} \tag{13}$$

The magnetic surfaces inside the plasma region are described by

$$Z = Z(X) - \sqrt{\lambda(R-R(X))^2 + \Delta^2}. \tag{14}$$

In this expression, we define a quantity

$$\Delta^2 = \frac{(\Psi - \Psi(X))}{\alpha}. \tag{15}$$

We also have

$$|\nabla\Psi| = 2\alpha[\lambda(\lambda+1)(R-R(X))^2 + \Delta^2]^{1/2}. \tag{16}$$

Note that Δ is a characteristic parameter denoting the proximity in the perpendicular direction to the separatrix $\Psi = \Psi(X)$. The above equations are very useful in calculating a series of surface integrals related to the peeling stability and transport analyses.[21–23] In the following, for simplicity, we consider the configuration with up–down symmetry, then we have

$$\begin{aligned} V'(\Psi) = \oint \frac{\mathrm{d}l}{B_p} &\approx 2\int_{R_{\rm in}}^{R_{\rm out}} \frac{R\mathrm{d}R}{\Psi_Z} = 2\int_{R_x-\delta}^{R_x+\delta} \frac{R\mathrm{d}R}{\Psi_Z} \approx -\frac{R_0^3 x_s}{\Psi_a\alpha}\int_0^\delta \frac{\mathrm{d}x}{\sqrt{\lambda x^2+\Delta^2}} \\ &= -\frac{R_0^3 x_s}{\Psi_a\alpha\sqrt{\lambda}}\ln\Big[\frac{\sqrt{\lambda\delta^2+\Delta^2}+\sqrt{\lambda}\delta}{\Delta}\Big] \approx -\frac{R_0^3 x_s}{\Psi_a\alpha\sqrt{\lambda}}\ln\Big(\frac{2\sqrt{\lambda}\delta}{\Delta}\Big), \end{aligned} \tag{17}$$

$$q(\Psi) \approx \frac{(FR_0/\Psi_a)}{\pi\alpha\sqrt{\lambda}R(X)}\ln\Big[\frac{\sqrt{\lambda\delta^2+\Delta^2}+\sqrt{\lambda}\delta}{\Delta}\Big] \approx \frac{q_0\sqrt{\eta}}{\pi\alpha x_s\sqrt{\lambda}}\ln\Big(\frac{2\sqrt{\lambda}\delta}{\Delta}\Big). \tag{18}$$

In the above expressions, δ is a small quantity denoting the departure of a point on the integral route from the X-point. We will see below that its value does not affect its physical results. Extending to any quantity, for $\Delta \to 0$, in the lowest approximation, we obtain $\langle A \rangle = A(X)$.

3. Diverted equilibrium configurations with nonzero edge current

For $p(\Psi)$ in Eq. (7) and $F^2(\Psi)$ in Eq. (8), the Grad–Shafranov equation (4) becomes

$$\frac{\partial^2 \Psi}{\partial R^2} - \frac{1}{R}\frac{\partial \Psi}{\partial R} + \frac{\partial^2 \Psi}{\partial^2 Z} = -\left(\frac{2\mu_0 p_0}{\Psi_a^2}R^2 + \frac{B_{t0}^2 R_0^2 a_2}{\Psi_a^2}\right)\Psi - \left(\frac{\mu_0 p_1}{\Psi_a}R^2 + \frac{B_{t0}^2 R_0^2 a_2}{2\Psi_a}\right). \tag{19}$$

By introducing

$$\bar{\Psi} = \Psi/\Psi_a,\ x = R/R_0,\ y = Z/R_0,\ \beta_a = 2\mu_0 p_0/B_{t0}^2,$$
$$\beta_1 = 2\mu_0 p_1/B_{t0}^2,\ \eta = \left(\frac{B_{t0}R_0^2}{\Psi_a}\right)^2, \tag{20}$$

equation (19) turns into its dimensionless form

$$\frac{\partial^2 \bar{\Psi}}{\partial x^2} - \frac{1}{x}\frac{\partial \bar{\Psi}}{\partial x} + \frac{\partial^2 \bar{\Psi}}{\partial y^2} + \eta[(a_2 + \beta_a x^2)\bar{\Psi} = -\frac{\eta}{2}(a_1 + \beta_1 x^2). \tag{21}$$

To solve the linear inhomogeneous partial differential equation (21), we assume a two-term separable solution as in Eq. (1) but now in dimensionless form

$$\bar{\Psi}(x, y) = f(x)\cos ky + g(x). \tag{22}$$

For the given k, we obtain two ordinary differential equations

$$\frac{\mathrm{d}^2 f}{\mathrm{d}x^2} - \frac{1}{x}\frac{\mathrm{d}f}{\mathrm{d}x} + [-k^2 + \eta(a_2 + \beta_a x^2)]f = 0, \tag{23}$$

$$\frac{\mathrm{d}^2 g}{\mathrm{d}x^2} - \frac{1}{x}\frac{\mathrm{d}g}{\mathrm{d}x} + [-k^2 + \eta(a_2 + \beta_a x^2)]g = -\frac{1}{2}\eta(a_1 + \beta_1 x^2). \tag{24}$$

The procedure to obtain solutions for both the homogeneous equation (23) and the inhomogeneous equation (24) is similar to our previous method.[3–5] However, because now we have an inhomogeneous term in Eq. (24), there are some differences between them. In the homogeneous case, i.e., for $a_1 = \beta_1 = 0$, we can freely select the maximum poloidal flux Ψ_a. However, now the physical values of these parameters will not be independent of each other, so we select an initial position x_1 (its value is related to the aspect ratio of the configuration) and assume the initial conditions of $f(x)$ and $g(x)$ as follows:

$$f(x_1) = 0, \quad f'(x_1) = 1.0, \tag{25}$$

$$g(x_1) = -1. \quad g'(x_1) = s_0. \tag{26}$$

For any set of parameters (η, β_a, α_2, β_1, α_1), we can numerically determine the functions $f(x)$ and $g(x)$ in region $x \geq x_1$; and suitably selecting the s_0 value, we can find that at some point x_s, the above two functions satisfy the following condition

$$f(x_s) + g(x_s) = 0. \tag{27}$$

If we select

$$y_s = \pi/k, \tag{28}$$

then we see that conditions (25) and (26) are just those the diverted configuration needs to satisfy

$$\frac{\partial \bar{\Psi}}{\partial x} = f'(x)\cos ky + g'(x) = 0,$$
$$\frac{\partial \bar{\Psi}}{\partial y} = -kf(x)\sin ky = 0.$$

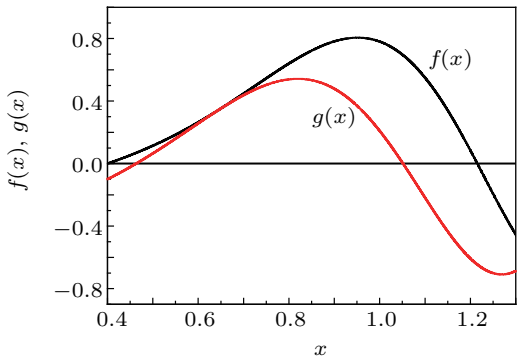


Fig. 1. (colour online) The two base functions required for constructing a model double-null diverted tokamak configuration. The corresponding parameters are: $\eta\beta_a = 50$, $\eta\beta_1 = 10$, $\eta\alpha_2 = -5$, $\eta\alpha_1 = -2$, $s_0 = 1.45613$, $x_s = 0.64828$, $\bar{\Psi}_x = -1.97 \times 10^{-6}$.

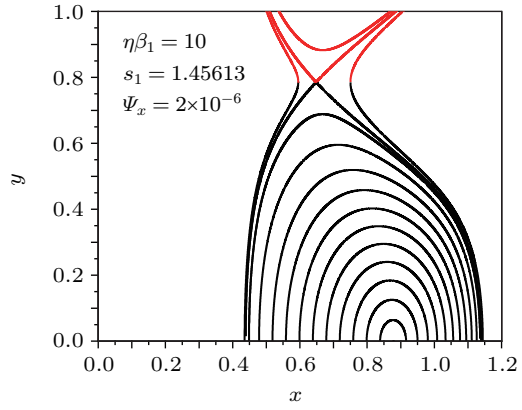


Fig. 2. (colour online) The double-null diverted tokamak configuration for the same parameters as those in Fig. 1.

In this paper, we mainly discuss tokamak configuration. For any given set of parameters ($\eta\beta_a$, $\eta\alpha_2$, $\eta\beta_1$, $\eta\alpha_1$, k, x_1), we solve Eqs. (23) and (24) under initial conditions (25) and (26) and adjust the value s_0 to satisfy condition (27), then a model double-null diverted configuration will be constructed. As an example, two base functions are shown in Fig. 1, and the corresponding diverted configuration is shown in Fig. 2.

3.1. Configurations compatible with pure PS current

Now we consider an interesting case where the edge current is a pure PS current. The parameters in the above cited configuration are not completely compatible with this case (the externally driven current equals zero at the X-point). So to study this pure PS current case, we need to further adjust the parameters $\eta\alpha_1$ and s_0 simultaneously. The corresponding configuration is shown in Fig. 3 with the two parameters as $\eta\alpha_1 = -4.59$, $s_0 = 1.29685$. Comparing Fig. 2 and Fig. 3, we find that the X-point position of the pure PS current case is a little more outwardly shifted and the diamagnetic (the negative value of $\eta\alpha_1$) is larger. The corresponding curves for the PS current density along the separatrix and the Ψ_{95} surface are shown in Fig. 4. We can see that at the position of the X-point ($x_s = 0.6777$), $j_\zeta^{\rm PS} = 0$.

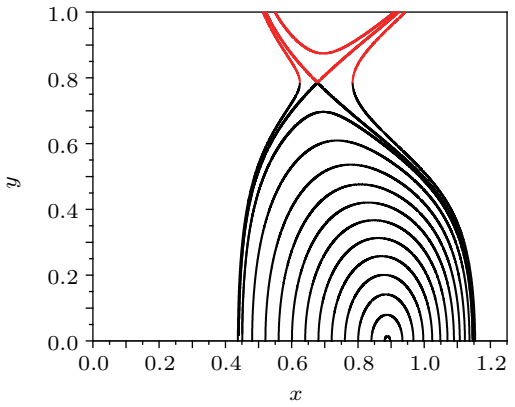


Fig. 3. (colour online) A double-null diverted tokamak configuration with pure PS edge current. The parameters are taken as: $\eta\alpha = -5$, $\eta\beta = 50$, $\eta\alpha_1 = -4.59$, $\eta\beta_1 = 10$, $s_0 = 1.29685$, $x_s = 0.6777$, $\eta = 374.3$, $\Psi_\mu = 1.3408$, $\Psi_x = -1 \times 10^{-5}$.

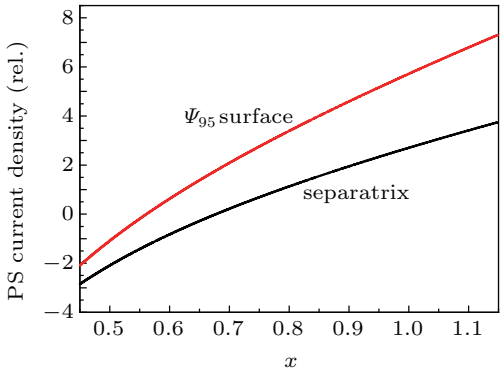


Fig. 4. (colour online) PS current density along the separatrix (lower) and Ψ_{95} surface (upper) for the configuration shown in Fig. 3.

Now we return to illustrate how to determine the value of the parameter $\eta = (B_{t0}R_0^2/\Psi_a)^2$. This can be found from the expression of the safety factor near the magnetic axis (the detail can be found in Refs. [3]–[5]).

$$\eta = (q_0 k x_m)^2 f(x_m)[f''(x_m) + g''(x_m)]. \tag{29}$$

We also show this value for $q_0 = 1$ in the corresponding configuration so that we can directly obtain the value of Ψ_a for a given magnetic field and the major radius:

$$\Psi_a = \frac{B_{t0}R_0^2}{\sqrt{\eta}}. \tag{30}$$

The present-day H-mode tokamak configuration usually permits a higher edge pressure gradient and correspondingly large edge PS current. This kind of configuration can be obtained by simultaneously increasing the edge pressure gradient parameter β_1, and adjusting the negative value of the diamagnetism parameter α_1, as well as the value of s_0. Figure 5 is an example, with the parameters indicated in its caption. In Fig. 6 we show the extended magnetic surfaces in the region very near the X-point. We can see that due to the current density at the X-point equal to zero, we have $\Psi_{RR}(X) = -\Psi_{ZZ}(X)$, i.e., $\lambda = 1$, and two lines across the X-point are perpendicular to each other.

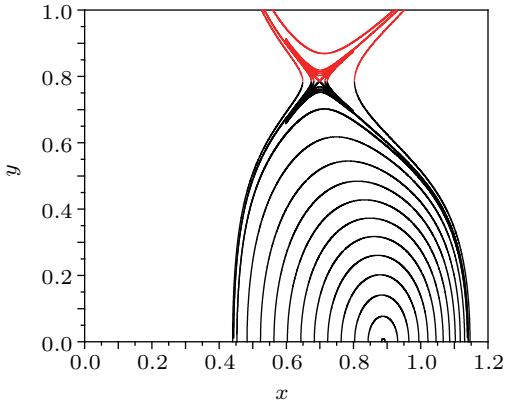


Fig. 5. (colour online) A configuration with larger edge PS current. The denser curves in the region near the X-point are calculated by the approximate equation (13). The parameters are taken as: $\eta\alpha_2 = -5$, $\eta\beta_a = 50$, $\eta\alpha_1 = -9.76$, $\eta\beta_1 = 20$, $k = 4$, $s_0 = 1.1149$, $x_s = 0.6987$, $\eta = 366.8$, $\Psi_x = 1.39 \times 10^{-5}$, $\Psi_a = 1.362$, $\Psi_{xx}(X) = -7.1225$, $\Psi_{yy}(X) = -7.1239$.

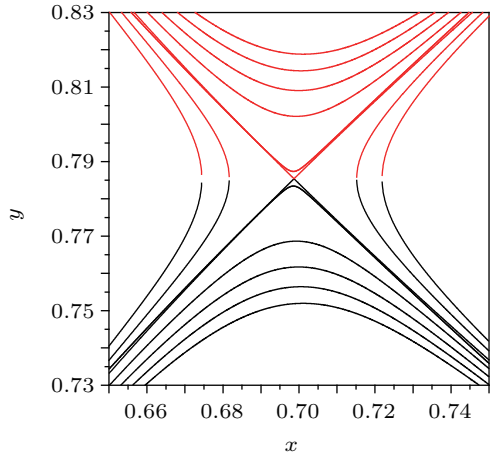


Fig. 6. (colour online) Extended magnetic surfaces near the X-point for the configuration shown in Fig. 5. Two lines across the X-point are orthogonal to each other ($\lambda = 1$).

3.2. Diverted equilibrium configurations with nonzero edge current

Now we consider the general case of nonzero Ohmic current, which is of importance for peeling-ballooning mode analysis.[21–23] The procedures are similar to the case of pure PS current. By selecting the parameter set to give nonzero edge current, i.e., let $\eta\alpha_1+\eta\beta_1 x_s^2 \neq 0$, we can obtain the corresponding configurations. Figures 7 and 8 are examples, and for each of them the corresponding parameters and equilibrium quantities are shown in each caption. Figure 9 shows the extended magnetic surfaces near the X-point for the configuration shown in Fig. 8. It is shown that due to the nonzero edge current, $\Psi_{xx}(X) \neq -\Psi_{yy}(X)$ or $\lambda \neq 1$, this leads to non-orthogonality of the two crossed lines at the X-point.

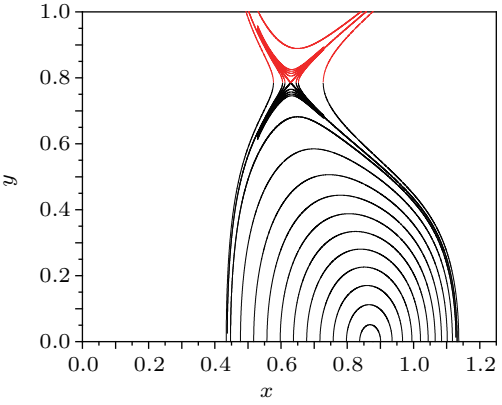


Fig. 7. (colour online) The configuration with nonzero edge current. In the region near the X-point, dense magnetic surfaces are obtained from approximate equation (13). The parameters are taken as: $\eta\alpha_2 = -5$, $\eta\beta_a = 50$, $k = 4$, $\eta\alpha_1 = 0$, $\eta\beta_1 = 10$, $s_0 = 1.56773$, $x_s = 0.629$, $\eta = 286.34$, $\Psi_x = 1.22 \times 10^{-6}$, $\Psi_a = 1.2126$, $\Psi_{xx}(X) = -7.008$, $\Psi_{yy}(X) = 5.032$.

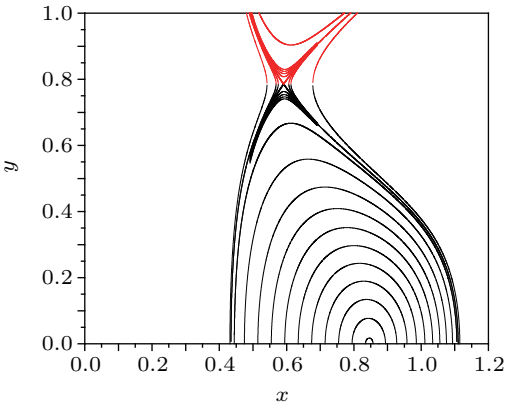


Fig. 8. (colour online) The configuration with a larger nonzero edge current. The denser curves in the region near the X-point are also from Eq. (13). The parameters are taken as: $\eta\alpha_2 = -5$, $\eta\beta_a = 50$, $\eta\alpha_1 = 5$, $\eta\beta_1 = 10$, $k = 4$, $s_0 = 1.8127$, $x_s = 0.5912$, $\eta = 225.63$, $\Psi_x = -6.4 \times 10^{-7}$, $\Psi_a = 1.0684$, $\Psi_{xx}(X) = -8.2386$, $\Psi_{yy}(X) = 3.9912$.

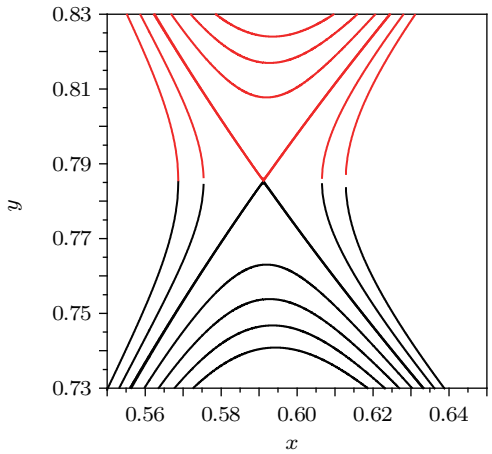


Fig. 9. (colour online) Approximate magnetic surfaces in the near X-point region for the configuration shown in Fig. 8. Two lines across the X-point are not orthogonal to each other ($\lambda = 2.06$).

4. Conclusions

Exact diverted tokamak equilibria with nonzero edge current are constructed by extending our previous semi-analytic method for equilibria with zero edge current. Double-null equilibria with up–down symmetry are considered, and the main differences in solving the procedure between cases with and without edge current are indicated. Configurations obtained in this way make it possible to calculate the X-point region very accurately so that we can consider several interesting physics processes around the separatrix, especially around the X-point region, such as the peeling-ballooning criterion,[21–23] and the collision-dominated transport of a diverted plasma,[18] etc.

References

[1] Burrel K H *et al.* 1992 *Plasma Physics Control Fusion* **34** 1859

[2] Suttrop W 2000 *Plasma Physics Control Fusion* **42** A1

[3] Bingren Shi 2008 *Plasma Physics Control Fusion* **50** 085006

[4] Bingren Shi 2009 *Plasma Physics Control Fusion* **51** 105008

[5] Bingren Shi 2011 *Nucl. Fusion* **51** 023004

[6] MaCarthy P J 1999 *Phys. Plasmas* **9** 3555

[7] Atanasiu C V, Gunter, Lackner K and Miron I G 2004 *Phys. Plasmas* **11** 3510

[8] Solov'ev L S 1967 *Zh. Eksp. Teor. Fiz* **53** 626 [*Sov. Phys. JETP* **26** (1968) 400]

[9] Zheng S B, Wootton A J and Solano E R 1996 *Phys. Plasmas* **3** 1176

[10] Weening R H 2000 *Phys. Plasmas* **7** 3654

[11] Bingren Shi 2006 *Phys. Plasmas* **12** 122504

[12] Bingren Shi 2004 *Plasma Physics Control Fusion* **46** 1105

[13] Srinivasan R, Avanash K and Kaw P K 2001 *Phys. Plasmas* **8** 4483

[14] Cerfon A J and Freidberg J P 2010 *Phys. Plasmas* **17** 032502

[15] Srinivasan R, Lao L L and Chu M S 2010 *Plasma Phys. Control Fusion* **52** 035007

[16] Guazzotto L and Friedberg J P 2007 *Phys. Plasma* **14** 112508

[17] Pfirsch D and SchlüterA 1962 *Max-Planck-Institute Report* MPI/PA/7/62

[18] Hazeltine R D and Hinton F L 1973 *Phys. Fluids* **16** 1883

[19] Catto P J and Simakov A N 2005 *Phys. Plasmas* **12** 012501

[20] Hahm T S and Diamond P H 1987 *Phys. Fluid* **30** 133

[21] Lortz D1975 *Nucl. Fusion* **15** 49

[22] Wilson H R, Connor J W, Field A R and Fielding S J 1999 *Phys. Plasmas* **6** 1925

[23] Connor J W, Hastie R J, Wilson H R and Miller R L 1998 *Phys. Plasmas* **5** 2687